NASA TN D-335

TECHNICAL NOTE

D-335

FULL-SCALE WIND-TUNNEL TESTS OF BLOWING BOUNDARY-LAYER CONTROL APPLIED TO A HELICOPTER ROTOR

By John L. McCloud III, Leo P. Hall,
and James A. Brady

Ames Research Center
Moffett Field, Calif.

NATIONAL AERONAUTICS AND SPACE ADMINISTRATION

WASHINGTON

September 1960

NATIONAL AERONAUTICS AND SPACE ADMINISTRATION

TECHNICAL NOTE D-335

FULL-SCALE WIND-TUNNEL TESTS OF BLOWING BOUNDARY-LAYER CONTROL APPLIED TO A HELICOPTER ROTOR

By John L. McCloud III, Leo P. Hall, and James A. Brady

SUMMARY

A full-scale wind-tunnel test was conducted of two boundary-layer-control applications to a 44-foot diameter helicopter rotor. Blowing from a nozzle near the leading edge of the blades delayed retreating blade stall. Results also indicated that delay of retreating blade stall could be obtained by cyclic blowing with a lower flow rate than that required for continuous blowing.

It was found that blowing applied through a nozzle at mid-chord had no effect on retreating blade stall.

INTRODUCTION

The maximum forward speed and the lifting capacity of a helicopter in forward flight can be limited by retreating blade stall. Retreating blade stall may be avoided by such means as increased rotor solidity or the use of high tip speeds. Recently, it has been shown (ref. 1) that a cambered airfoil section by delaying retreating blade stall enabled a rotor with cambered blade sections to achieve either higher lift in forward flight or higher maximum forward speeds than a similar rotor with symmetrical blade sections. Boundary-layer control can increase stalling angles and lifts of airfoil sections so it might be expected that it could delay retreating blade stall. Two applications of boundary-layer control to a helicopter rotor were used in the present investigation. These applications involve blowing on the upper surface of the blades, and were differentiated by the chordwise location of the blowing nozzles, that is, near mid-chord and near the leading edge.

The two three-bladed rotors (44 feet in diameter) were tested in the Ames 40- by 80-Foot Wind Tunnel in order to determine their stall boundaries and the effects of the boundary-layer-control applications on these boundaries. The tests simulated forward flight conditions corresponding to an advance ratio range of approximately 0.34 to 0.46 at a rotor tip speed of 450 feet per second.

A limited amount of testing was done with blowing air cycled in an attempt to reduce the amount of blowing air required.

Representative data are presented herein to show how retreating blade stall was detected, and the stall boundaries thus determined are compared with the stall boundaries of similar rotors without boundary-layer control reported in reference 1.

NOTATION

Positive directions of forces and moments are shown in the following sketch:

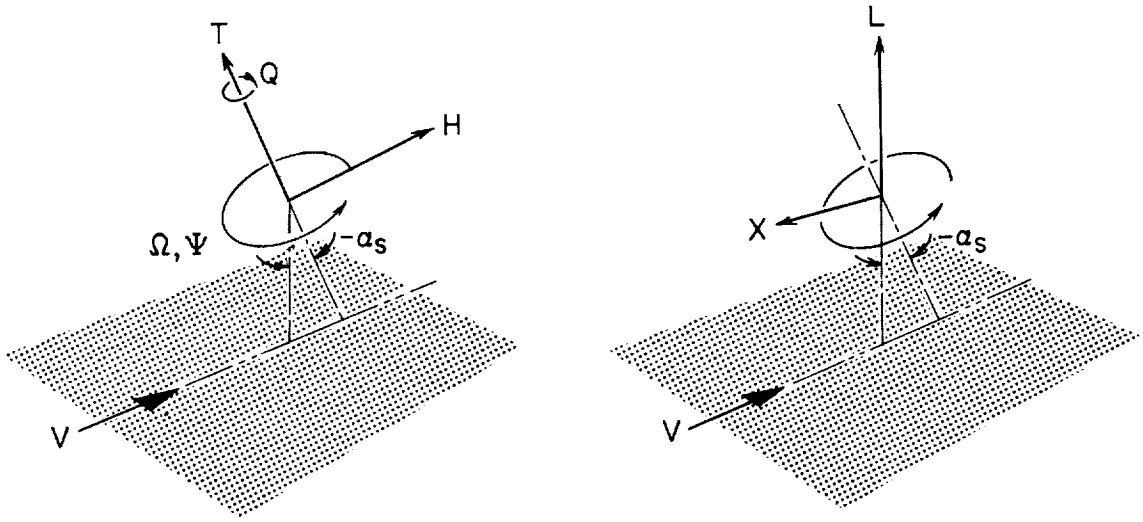

b	number of blades
c	chord of blades, ft
C_{L_R}	rotor lift coefficient, $\frac{L}{\rho(\Omega R)^2 \pi R^2}$
C_P	power coefficient, $\frac{P}{\rho(\Omega R)^3 \pi R^2}$
C_Q	torque coefficient, $\frac{Q}{\rho(\Omega R)^2 \pi R^3}$

C_X	longitudinal-force coefficient, $\frac{X}{q\pi R^2}$
C_{X_R}	rotor longitudinal-force coefficient, $\frac{X}{\rho(\Omega R)^2\pi R^2}$
$\bar{C}_\mu$	rotor boundary-layer-control momentum coefficient (see appendix)
c_μ	section boundary-layer-control momentum coefficient (see appendix)
F	boundary-layer-control distribution factor (see appendix)
f	equivalent parasite drag area, sq ft
HP	horsepower
L	lift force, lb
p_r	blade root pressure, psia
P	shaft power, lb-ft/sec
q	dynamic pressure, $\frac{1}{2}\rho V^2$, lb/sq ft
Q	shaft torque, lb-ft
R	rotor radius, ft
r	radial station, ft
V	airspeed, ft/sec
$\frac{V}{\Omega R}$	advance ratio
W	boundary-layer-control air-flow rate, lb/sec
X	longitudinal force, lb
x	ratio of radial station to blade radius, $\frac{r}{R}$
α_s	shaft angle, deg (equivalent to control axis inclination)
$\theta_{0.75}$	blade-section pitch angle; angle between line of zero lift of blade section and plane perpendicular to shaft axis measured at the 0.75 radius station, deg

ρ mass density of air, slugs/cu ft

Ψ azimuth of blade measured counterclockwise from downwind position, deg

Ω angular velocity of rotor, radians/sec

APPARATUS

Rotor Support and Drive System

The rotors were supported and driven in the wind tunnel by the same tripod and drive system used during the previous rotor investigation (ref. 1). As in that investigation, no windshields or fairings were provided to shield the rotor support from the air stream. The rotor support is shown in figure 1, reproduced from reference 1.

Boundary-Layer-Control Air Supply

Air for the boundary-layer-control applications was supplied by an aircraft supercharger driven by an electric motor mounted just below the tunnel floor on the tunnel balance frame. The air was ducted through an 8-inch orifice meter into the right angle gear box of the rotor drive and then up through the rotor drive shaft to a manifold just above the rotor hub. The manifold is visible in figure 2 and shown in more detail in figure 3(a). The air entered the blades through flexible hoses connecting the manifold to the intake horns on the trailing edge of the blade spar root as shown in figure 2. The hollow spars of the rotor blades duct the air to the nozzles.

A few test runs were made with a cyclic valve for the boundary-layer-control air flow. The valve is shown in figure 3(b). The contoured inner block was held stationary, and the rotation of the manifold performed the cyclic opening and closing. Each blade received boundary-layer-control air for 120° of rotation, beginning at $\Psi = 210°$ and ending at $\Psi = 330°$ azimuth positions (measured from downwind position).

Rotor Hub and Blades

The rotor hub was the same fully articulated hub described in reference 1. The more pertinent hub dimensions are given in a subsequent table.

Both sets of boundary-layer-control blades had identical twists and plan forms, and employed the same general construction and leading-edge cambered airfoil section of the cambered blades of reference 1. Table I lists the airfoil section coordinates. The air intakes and nozzle postions are shown in the plan-form sketches of figure 4.

The leading-edge boundary-layer-control blades had a nozzle formed by a 0.016-inch-thick stainless-steel sheet wrapped around wood fairing strips as shown in figure 5. The nozzle opening was at about 8-1/2-percent chord and its opening height was maintained by shims of various thickness. These heights are indicated in figure 4. The nozzle height and sheet thickness increased the upper surface ordinates between the 1.5 and 8.5 percent chord stations.

The mid-chord blades had 32 nozzles spaced as shown in figure 4. These nozzles were formed by short plastic ducts bonded to the rear of the blade spar as shown in figure 6. The nozzle openings were of essentially equal area (i.e., about 2.5 inches long, and 0.1 inch high). They were spaced about 0.5 inch apart along the 44.5-percent chord line. Further data concerning the rotor hub and blade are given below.

	Leading-edge nozzle blade	Mid-chord nozzle blade
Flapping hinge offset, in.	4.60	4.60
Lagging hinge offset, in.	13.30	13.30
Solidity	0.0645	0.0645
Twist, deg	-7	-7
Weight per blade, lb	131	135
Radial station at blade c.g., in.	119.8	120.0

INSTRUMENTATION

The steady aerodynamic forces and moments were measured by the six-component wind-tunnel balance system. Rotor rotational speed was determined from rotational period measurement. (An electronic counter measured the time between pulses of a magnetically actuated switch mounted adjacent to the rotor shaft.) Blade pitching moments were sensed by resistance-type strain gages incorporated in the blade angle locking links. A rotary transformer provided flapping motion data for one of the blades. Electrical power and the data signals were led to and from the rotor hub through a multiple channel slip ring assembly visible in figure 2. These

data were continually monitored during the test program. Pressure and temperature measurements were made of the boundary-layer-control air at the previously mentioned orifice meter.

TEST PROCEDURE

To define a boundary of retreating blade stall, individual test runs were made at essentially constant advance ratios ($V/\Omega R$) with rotor shaft angle as the test variable. The rotor shaft angle was increased (i.e., became less negative) until two or three data points within the stall region were obtained, as indicated by the monitored blade pitching-moment signals. Runs were repeated for several different flow rates of the boundary-layer-control air, and for several advance ratios in the region of interest. The ranges of the tests are summarized as follows:

Rotor	Leading-edge blowing	Mid-chord blowing
Flow rate, lb/sec	1 to 3 lb	1-1/2 to 2-1/2
Blade angle, $\theta_{0.75}$	13° and 15°	15°
Advance ratio, approximately	0.34 to 0.46	0.34 to 0.39
Tip speed	450 fps	450 fps
Disk loading	0 to 3.5 psf	0 to 3.5 psf
Horsepower	0 to 525	0 to 485

Corrections to Data

The only corrections applied to these data are the air load tares (determined during previous investigation) for the rotor tripod support and the normal corrections for determining the tunnel air-flow velocity. The support tares do not include any effects of rotor operation. However, since the support is composed of circular tubes and is therefore nonlifting, it is believed the effect of the rotor operation on the tares is small and that the data as presented represent a conservative measure of the rotor forces. As in the previous investigation, no tunnel-wall corrections have been applied because of the uncertainty of their validity. In any case, the presence or absence of corrections should not affect the value of the data for purposes of comparing these boundary-layer-control applications.

The shaft torque and shaft power coefficients given in this report are based on the measurement of the tunnel balance frame reaction forces. These coefficients include the centrifugal pumping and jet reaction torques of the boundary-layer-control air flow which would exist for all rotors of this type.

RESULTS AND DISCUSSION

Determination of Retreating Blade Stall

A 3 8 0

It has been shown in reference 1 that the primary effect of retreating blade stall appears in the variation of rotor torque coefficient with shaft angle of attack. Further effects of stall appear as a change in character of the blade pitching moments as the blades pass the region of 270° to 360° azimuth position. These criteria have again been used to detect stall and hence to determine stall boundaries for the rotors.

Leading-Edge Boundary-Layer Control

Figure 7 shows some of the torque coefficient variations with shaft angle of the leading-edge boundary-layer-control rotor. The corresponding flow rates are given for each test run.

The filled symbols denote stalled conditions based on the torque criteria, and the flags denote conditions for which blade pitching-moment records indicated the presence of stall. Some typical blade pitching-moment traces are shown in figure 8. Figures 7 and 8 indicate how the onset of stall was determined; the stall boundaries were defined by the corresponding rotor lift and advance ratio values.

Specifically, lift coefficients for the last unstalled and first stalled point of operation (unfilled and filled symbols) are plotted against advance ratio. In figure 9 bands separating the filled and unfilled symbols thus define the stall boundaries of the rotor. Flagged symbols again denote stall indicated by blade pitching-moment traces.

It can be seen that for each flow rate or momentum coefficient a separate stall boundary results, with corresponding lift coefficient increases with increasing momentum coefficient. The momentum coefficient $\bar{C}_\mu$ is a dimensionless measure of the boundary-layer-control air flow and is defined in the appendix of this report. Figure 9 includes data obtained for both blade angle settings ($\theta_{0.75} = 13^\circ$ and 15°) and, as was found in reference 1, there is no significant change in the rotor lift coefficient at the stall boundary due to blade angle setting for the conditions tested.

The $\theta_{0.75} = 15^\circ$ data are limited to advance ratios of about 0.34 and 0.40. Attempts to operate the rotor at the higher advance ratios with this blade angle setting produced blade flapping motions approaching the mechanical limits of the test equipment; hence the stall boundary could not be reached.

The longitudinal force coefficients C_X which occurred at the highest stall boundary of figure 9 are shown in figure 10. Since the longitudinal force requirement for level flight is determined by the fuselage drag f (i.e., $C_X = f/\pi R^2$), the stall boundary of the rotor would not be affected by fuselage drag loadings which are within the range of the longitudinal force coefficients of these tests.

Since the leading-edge boundary-layer control was effective in delaying retreating blade stall, it was of interest to see if the required flow rates could be reduced. A few exploratory runs were made therefore using the previously described cyclic valve. The valve was positioned so that the boundary-layer-control air could enter the blades as they traversed downwind (approximately 210° to 330° azimuth positions). Again, increasing the air-flow rate increased the lift-coefficient values of the stall boundary as shown in figure 11. For about one-half the flow rate, cyclic blowing produced about the same lift-coefficient boundaries as did continuous blowing.

Tests were made with the valve facing the rear, advancing, and in the forward quadrants; however, the stall boundary was not affected for these valve positions. It is possible that greater savings in the air-flow rate might be realized by adjustment of the azimuth positions at which the valve opens and closes.

Mid-chord Boundary-Layer Control

The torque coefficient variations with shaft angle for the mid-chord boundary-layer-control rotor are shown in figure 12. Again filled and flagged symbols denote stalled conditions based on the torque and blade pitching-moment criteria. Similar figures were used to determine the presence of stall. Lift-coefficient values corresponding to the last unstalled and first stalled (unfilled and filled symbols, respectively) are plotted to define the stall boundaries. Figure 13 shows these lift-coefficient values, and it can be seen that increasing the boundary-layer-control air-flow rate did not significantly alter the stall boundary of the rotor. Inasmuch as no beneficial effects of mid-chord blowing were found, no further tests of this rotor were conducted.

Comparison of Leading-Edge Boundary-Layer-Control Rotor With Symmetric and Cambered Rotor Blades

The stall boundaries of the symmetric and cambered rotors of reference 1 are shown in figure 14 together with the boundaries for the leading-edge boundary-layer-control rotor. It can be seen that at the lowest momentum coefficient, the boundary-layer-control rotor has a lower stall boundary than the symmetric rotor but, at the highest momentum coefficient tested, its stall boundary exceeds that of the cambered rotor. As noted in the description of the rotors, when the blowing slot was incorporated, the rotor leading edge was distorted. This may have caused large reductions in the stall boundaries and prevented the present tests from showing the full gains possible with leading-edge blowing. Nevertheless, the improvement in the stall boundary above that for the cambered rotor represents an increase in speed and lift which could be realized within the longitudinal force coefficient range, hence fuselage drag range, shown in figure 10. An increase in lift or forward speed would, of course, require additional power.

The determination of the additional power required to utilize the speed gains noted requires interpolation and extrapolation of the data obtained for defining the stall boundaries, and the resulting power requirements are of questionable accuracy because of this procedure. This has been done, however, to illustrate the magnitude of power increments involved. Figure 15 shows some shaft power variations with advance ratio for a $C_{LR} = 0.0061$ and longitudinal force coefficients of 0.0199, 0.0131, and 0.0065 (i.e., fuselage drag areas of $f = 30$, 20, and 10 sq ft, respectively). Noted on this figure are the advance ratios for stall (for $C_{LR} = 0.0061$) for the symmetric, cambered, and leading-edge boundary-layer-control blades (the latter for a $\bar{C}_{\mu} = 0.0033$). It can be seen that for the lowest fuselage drag loading, the power coefficient increases from 0.00037 at the symmetrical blade stall boundary to 0.00073 at the stall boundary for the leading-edge boundary-layer-control rotor. The corresponding increase in advance ratio is from 0.32 to 0.46. For the C_X needed for higher fuselage drag loadings even greater power increments would be required. These power increases are predominantly caused by the power requirements associated with the fuselage drag. This figure illustrates the need to keep fuselage drag loadings low if speed gains due to boundary-layer control or camber are to be obtained with reasonable power increases.

It is possible to make some comparisons of the torque characteristics with a minimum of cross plotting to demonstrate the order of magnitude of possible torque differences. Figure 16 shows lift against shaft torque and lift against longitudinal force coefficients for the boundary-layer-control application together with similar variations from reference 1 for the rotor with symmetric and with cambered blades. It can be seen that for lift and longitudinal forces below the stall boundaries, the

boundary-layer-control rotor torque ranges from 4 to 10 percent greater than the rotor with symmetric blades. Part of this difference may be related to the drag and windage torque of the flexible boundary-layer-control air ducts in the hub (see fig. 2), and the remainder may be due to the increased longitudinal force being produced. Within the accuracy of these data, rotor torque requirements were not affected by boundary-layer-control air flow except wherein stall was delayed.

Power Requirements for Boundary-Layer-Control Air Flow

"Air horsepower" requirements have been calculated for the test flow rates, assuming adiabatic compression from the tunnel static pressure to the static pressure at the blade root inlet. These inlet pressures were calculated from measurements made at the orifice meter during the tests and from appropriate duct losses based on measurements made during static tests. The calculated air horsepower and blade inlet pressures are shown in figure 17 for both continuous and cyclic air flows. For the test conditions shown in figure 11, continuous blowing required 38 and 75 air horsepower whereas cyclic blowing required only 23 and 35 air horsepower. The equivalent power coefficients are also shown and it may be noted that although these coefficients are significant, they are small relative to the power increments necessary for the high forward speeds indicated in figure 15.

CONCLUSIONS

The results of an investigation made to determine the effects of blowing boundary-layer control applied to a helicopter rotor with cambered blades indicate the following conclusions:

1. The retreating blade stall boundary can be delayed significantly in the advance ratio range of 0.3 to 0.46 by blowing near the leading edge of the rotor blades.

2. Cyclic blowing in the retreating blade region was effective in reducing the flow rate requirements for boundary-layer control to about one half of that required with continuous blowing on all three blades.

3. No change in the stall boundary was obtained with blowing applied through a mid-chord nozzle for the range of flow rates investigated.

4. In order to obtain significant improvements in forward speed with boundary-layer control, fuselage drag must be low to avoid large power increases.

Ames Research Center
National Aeronautics and Space Administration
Moffett Field, Calif., June 30, 1960

A
3
8
0

APPENDIX

THE MOMENTUM COEFFICIENT FOR ROTORS

To provide a dimensionless measure of the amount of boundary-layer control applied to the rotor, it was deemed desirable to define a parameter which relates the blowing-air flow rate with the geometry and operating conditions of the rotor. The parameter selected for this purpose was a dimensionless measure of the momentum of the boundary-layer-control air flow defined below:

$$\overline{C}_{\mu} = \frac{2(W/g)V_j}{\rho(\Omega R)^2 \pi R^2 \sigma}$$

A 3 8 0

where

$\frac{W}{g}$ mass flow rate of boundary-layer-control air supplied, slugs/sec

V_j boundary-layer-control air jet velocity, ft/sec

σ rotor solidity, $bc/\pi R$

It was also desirable to determine the local two-dimensional momentum coefficient c_μ used in airfoil investigations. This coefficient may be expressed as follows:

$$c_{\mu} = \frac{wv_j}{qgc}$$

where

w boundary-layer-control air-flow rate per unit span, lb/sec/ft

v_j boundary-layer-control jet velocity assuming isentropic expansion to free-stream pressure, ft/sec

q local free-stream dynamic pressure, $\frac{\rho U^2}{2}$, lb/ft^2

g acceleration of gravity 32.2 ft/sec^2

c airfoil chord, ft

ρ free-stream density, $slugs/ft^3$

U local stream velocity, ft/sec

The rotor momentum coefficient $\overline{C}_\mu$ can be converted to a local section momentum coefficient c_μ by means of a factor F such that

$$c_\mu = F\overline{C}_\mu$$

hence

$$F = \frac{(wv_j/WV_j/bR)}{(U/\Omega R)^2}$$

For the present investigation the value of F has been calculated for the 270° azimuth position (the position where boundary-layer control would be expected to be of the greatest benefit). It was also necessary to make the following assumptions in computing F:

A
3
8
0

1. The local boundary-layer-control air-flow rate was proportional to the ratio of the local nozzle area to the total nozzle area of the blades.

2. The local jet velocity was the same at all spanwise stations and equal to the jet velocity calculated on the basis of isentropic expansion to free-stream static pressure.

3. The local stream velocity was the rotational velocity minus the free-stream velocity, that is, $U = (x\Omega R - V)$.

Radial distributions of F for $\Psi = 270°$ are shown in figure 18 for three advance ratios. Scales for the corresponding section momentum coefficients c_μ for three values of $\overline{C}_\mu$ are on the right of the figure. For example, the 0.9 radial station has F values from 12 to 19 for the advance ratios shown; hence, the c_μ values for a $\overline{C}_\mu$ of 0.0033 are between 0.035 and 0.060. Unpublished two-dimensional data for an NACA 23012 airfoil section with a boundary-layer-control nozzle at 10-percent chord shows increases in maximum section lift coefficient from 1.4 for no blowing to 1.6 to 2.0 for c_μ values of 0.035 to 0.060.

REFERENCE

1. McCloud, John L. III, and McCullough, George B.: Wind-Tunnel Tests of a Full-Scale Helicopter Rotor With Symmetrical and With Cambered Blade Sections at Advance Ratios From 0.3 to 0.4. NACA TN 4367, 1958.

TABLE I.- COORDINATES OF THE CAMBERED BLADE SECTION

[Stations and ordinates given in percent of airfoil chord.]

Station	Upper surface	Lower surface
0	0	0
1.25	2.35	-1.64
2.5	3.30	-2.17
5.0	4.67	-2.69
7.5	5.60	-2.98
10	6.22	-3.22
15	7.00	-3.58
20	7.38	-3.75
25	7.57	-3.93
30	7.57	-4.04
40	7.21	-4.17
50	6.46	-3.96
60	5.55	-3.49
70	4.41	-2.87
80	3.13	-2.11
90	1.71	-1.18
95	.93	-.67
100	.13	-.13
Leading-edge radius: 1.35-percent airfoil chord		

A
3
8
C

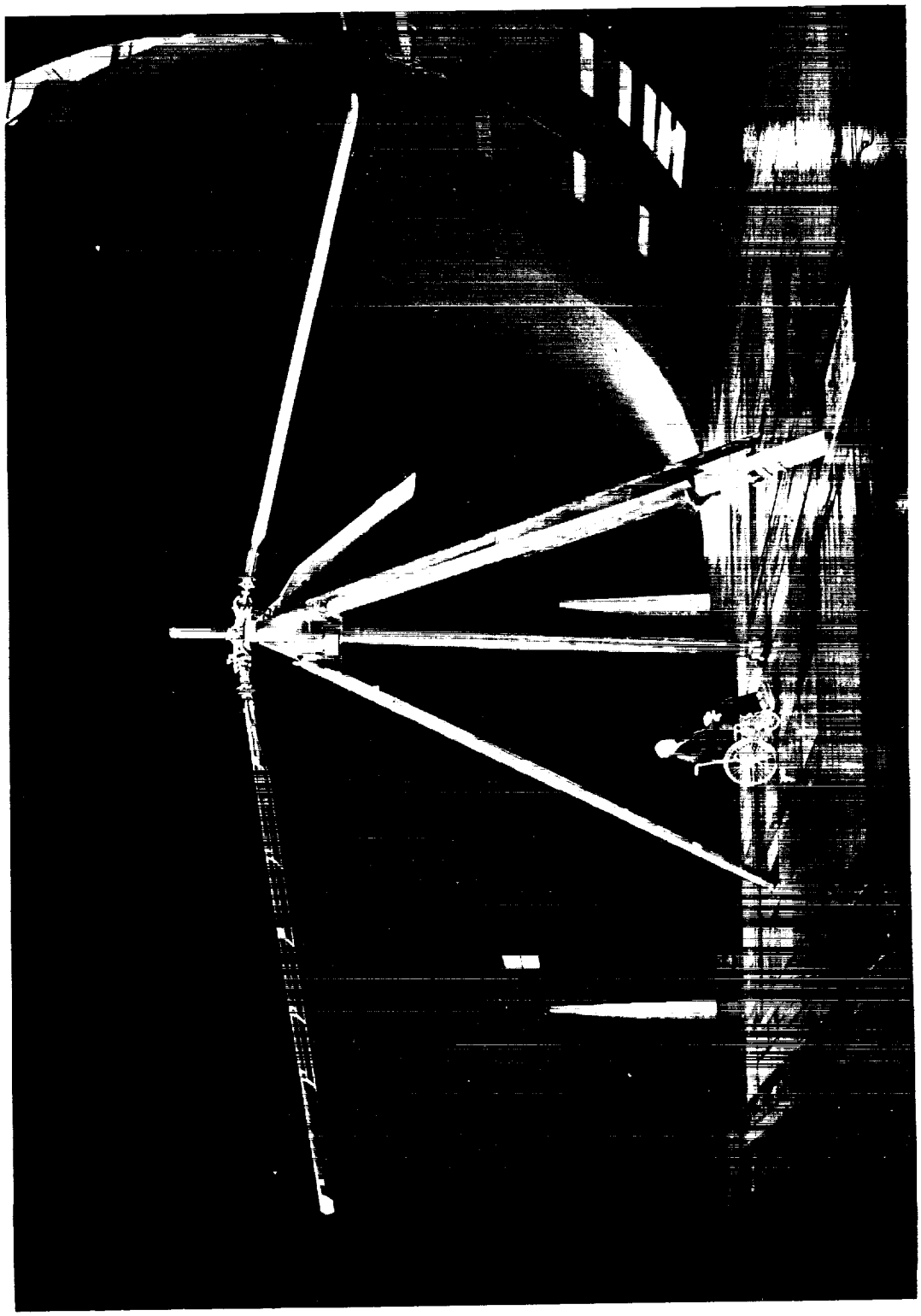

A-22383

Figure 1.- Helicopter rotor and support mounted in the wind tunnel.

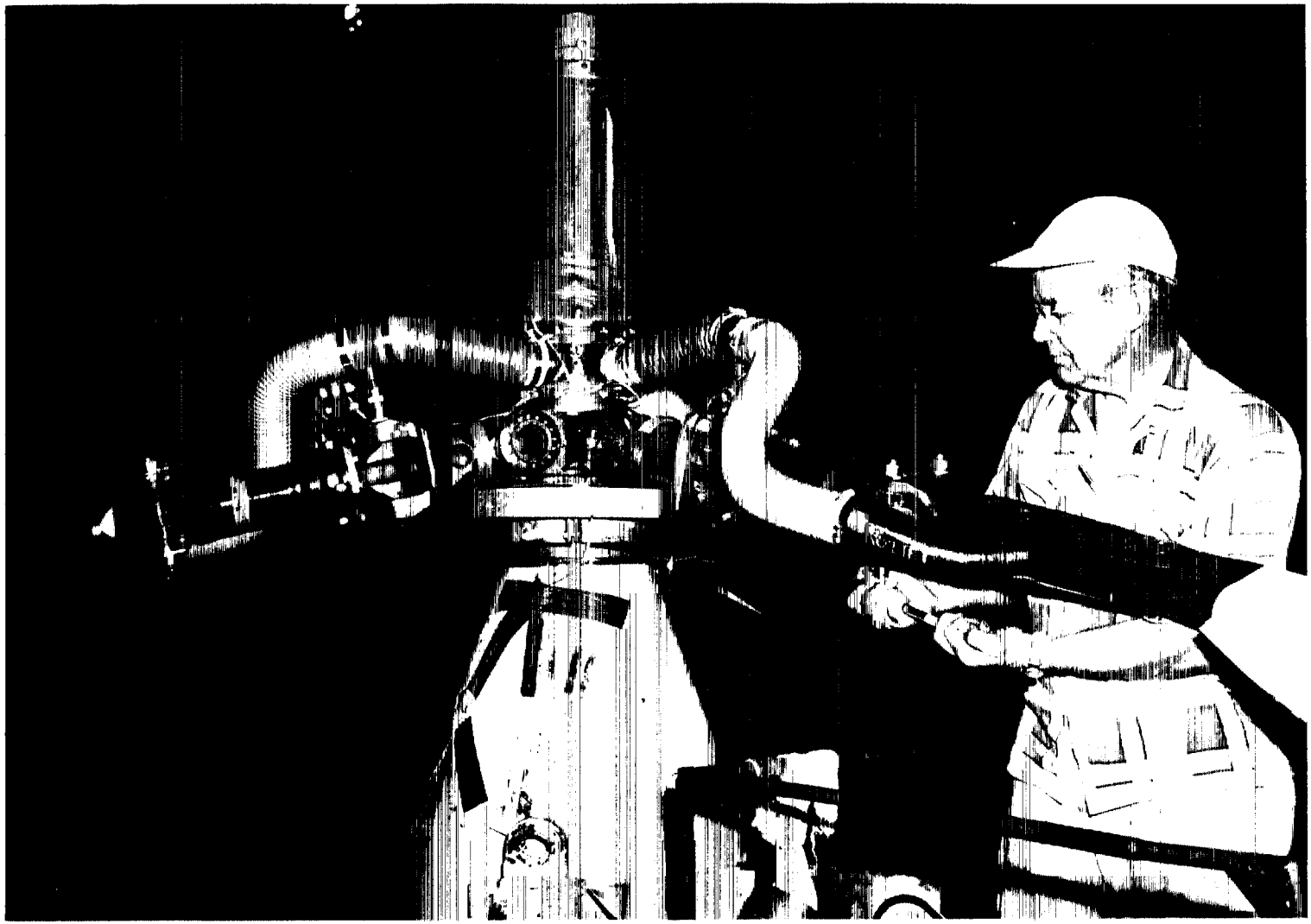

A-25429

Figure 2.- Photograph of rotor hub showing boundary-layer-control ducting to blades.

A-25305

(a) Manifold alone.

A-25304

(b) Manifold with valve.

Figure 3.- Photographs of boundary-layer-control air manifold.

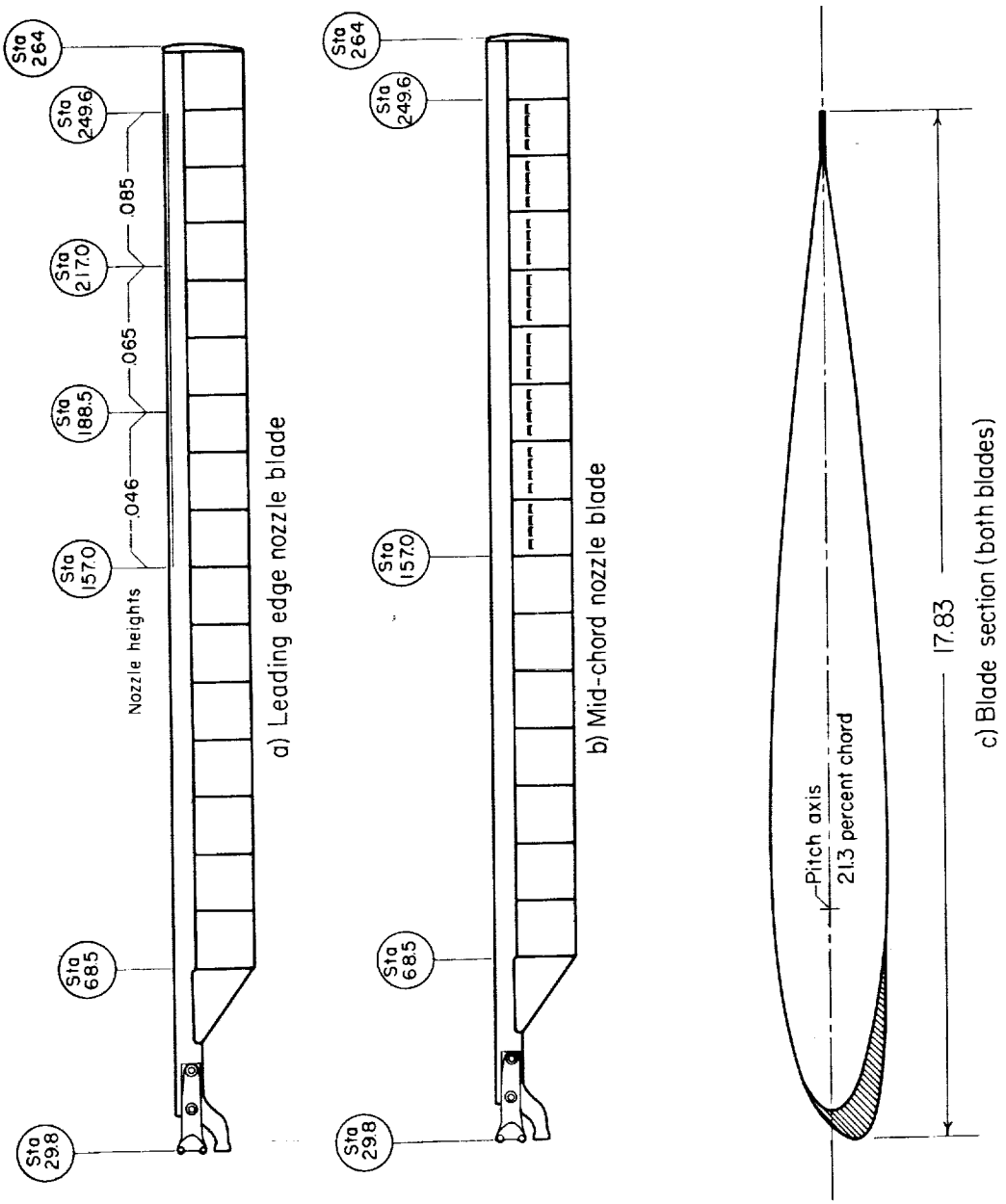

Figure 4.- Sketch of blade plan form and airfoil section.

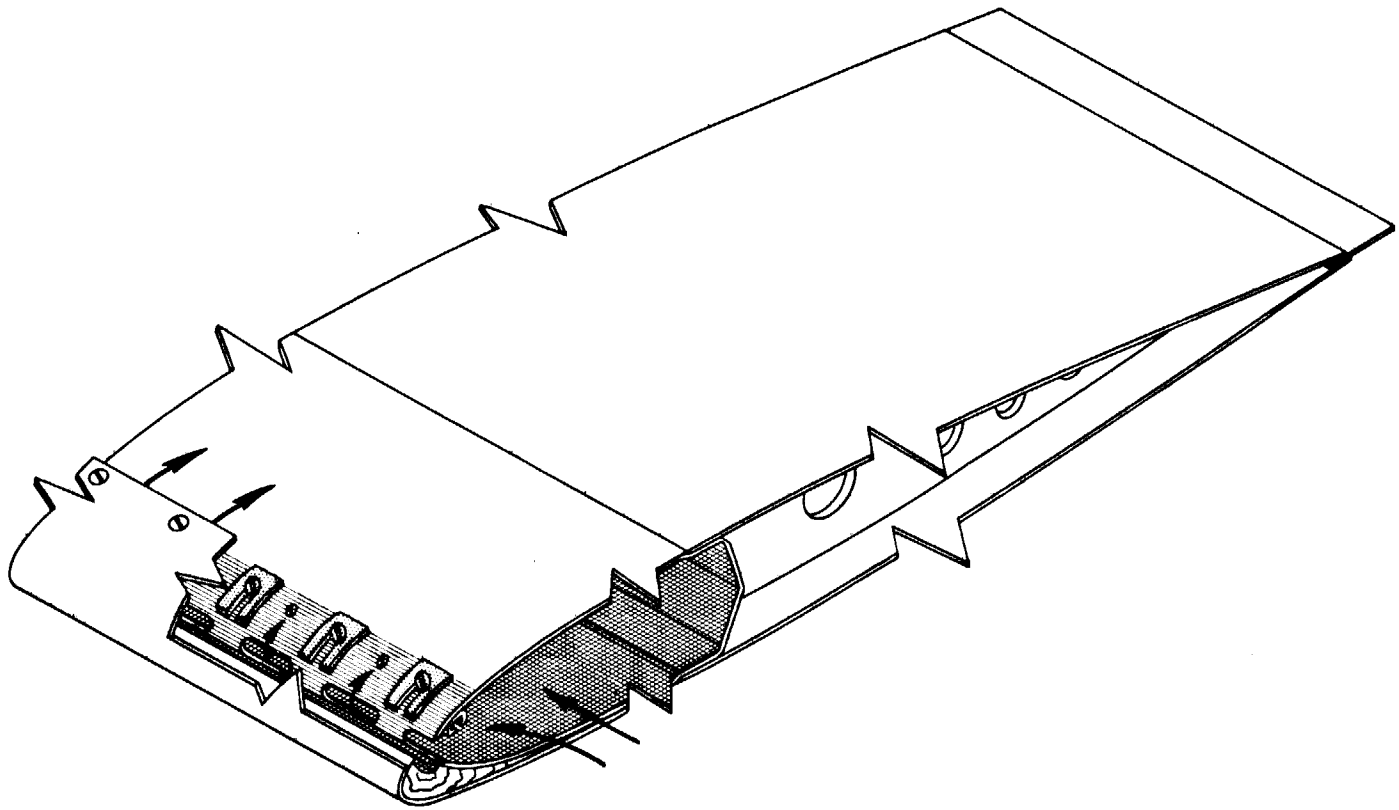

Figure 5.- Schematic drawing of leading-edge boundary-layer-control nozzle.

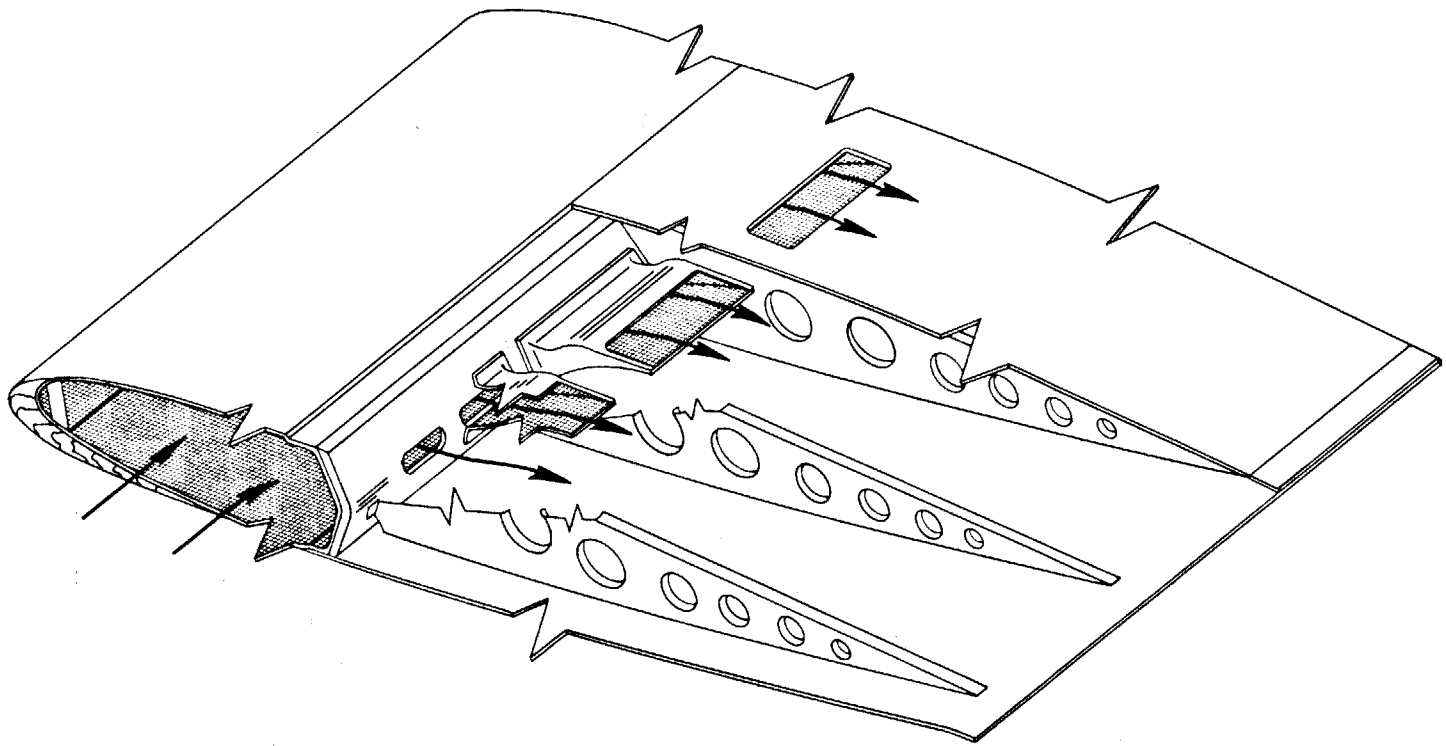

Figure 6.- Schematic drawing of mid-chord boundary-layer-control nozzle.

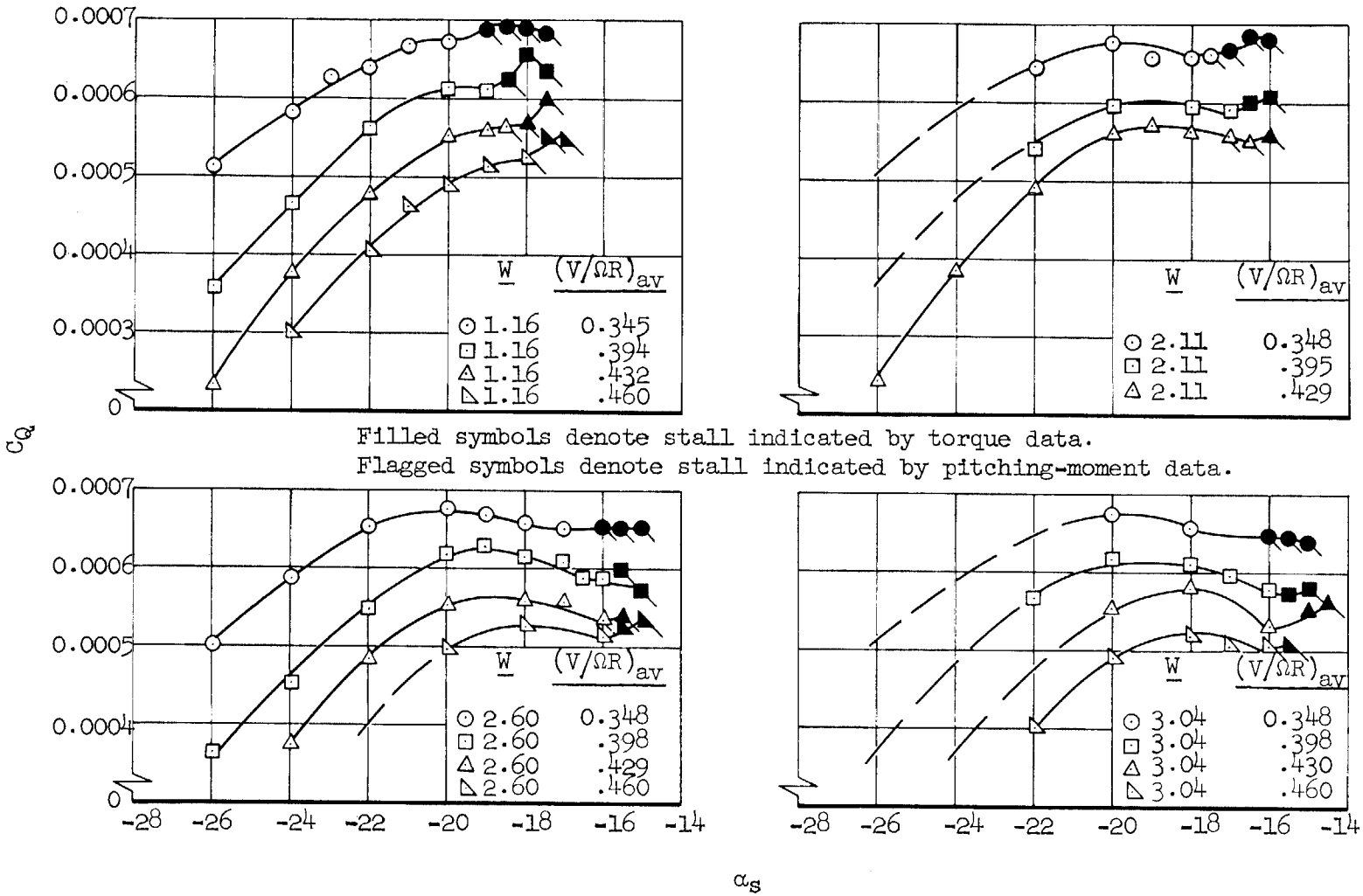

Figure 7.- Torque variations for the leading-edge boundary-layer control rotor; $\theta_{0.75} = 13°$.

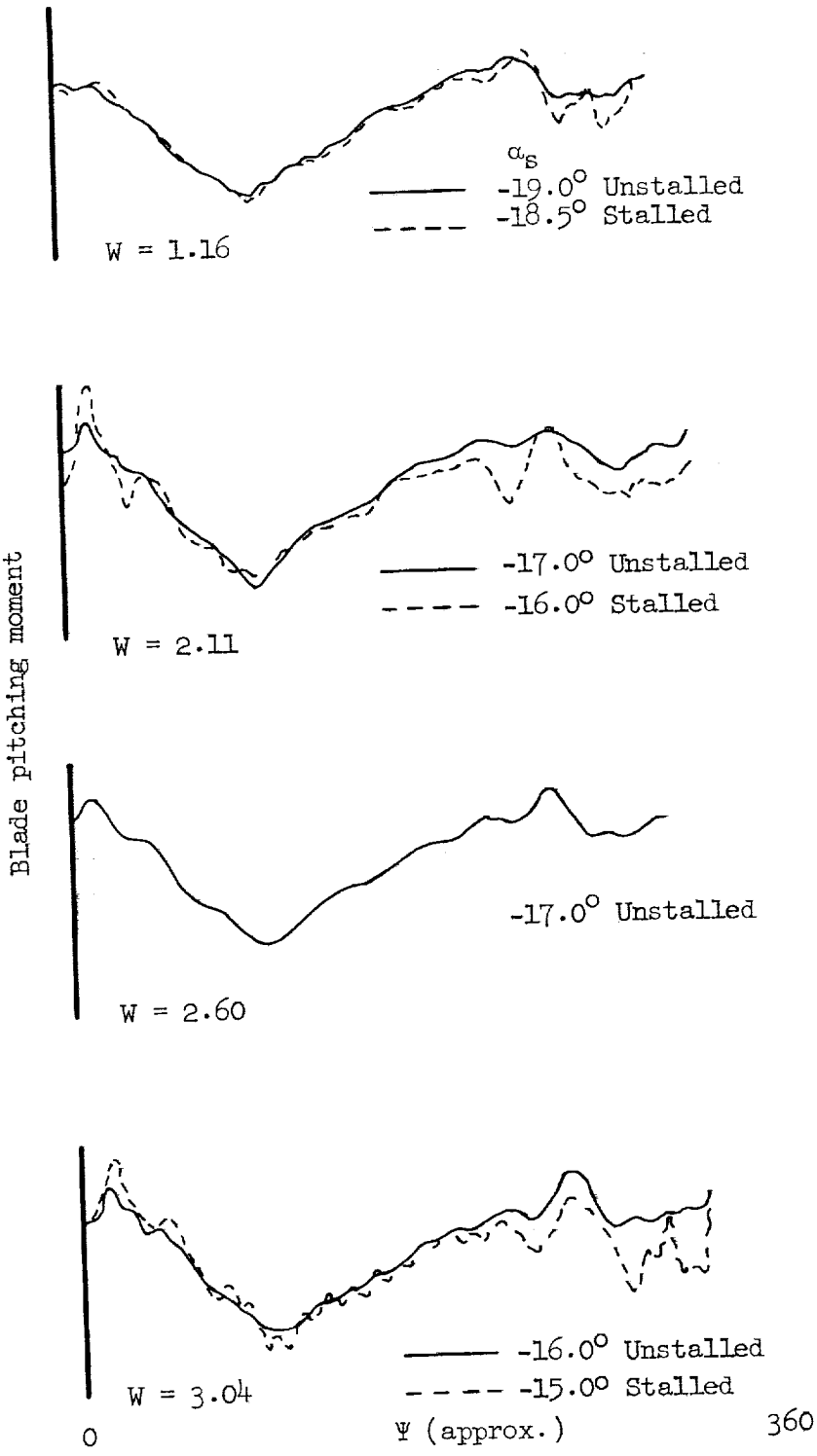

Figure 8.- Typical blade pitching-moment traces for blades with leading-edge boundary-layer control; $\theta_{0.75} = 13^\circ$; $(V/\Omega R)_{av} = 0.396$.

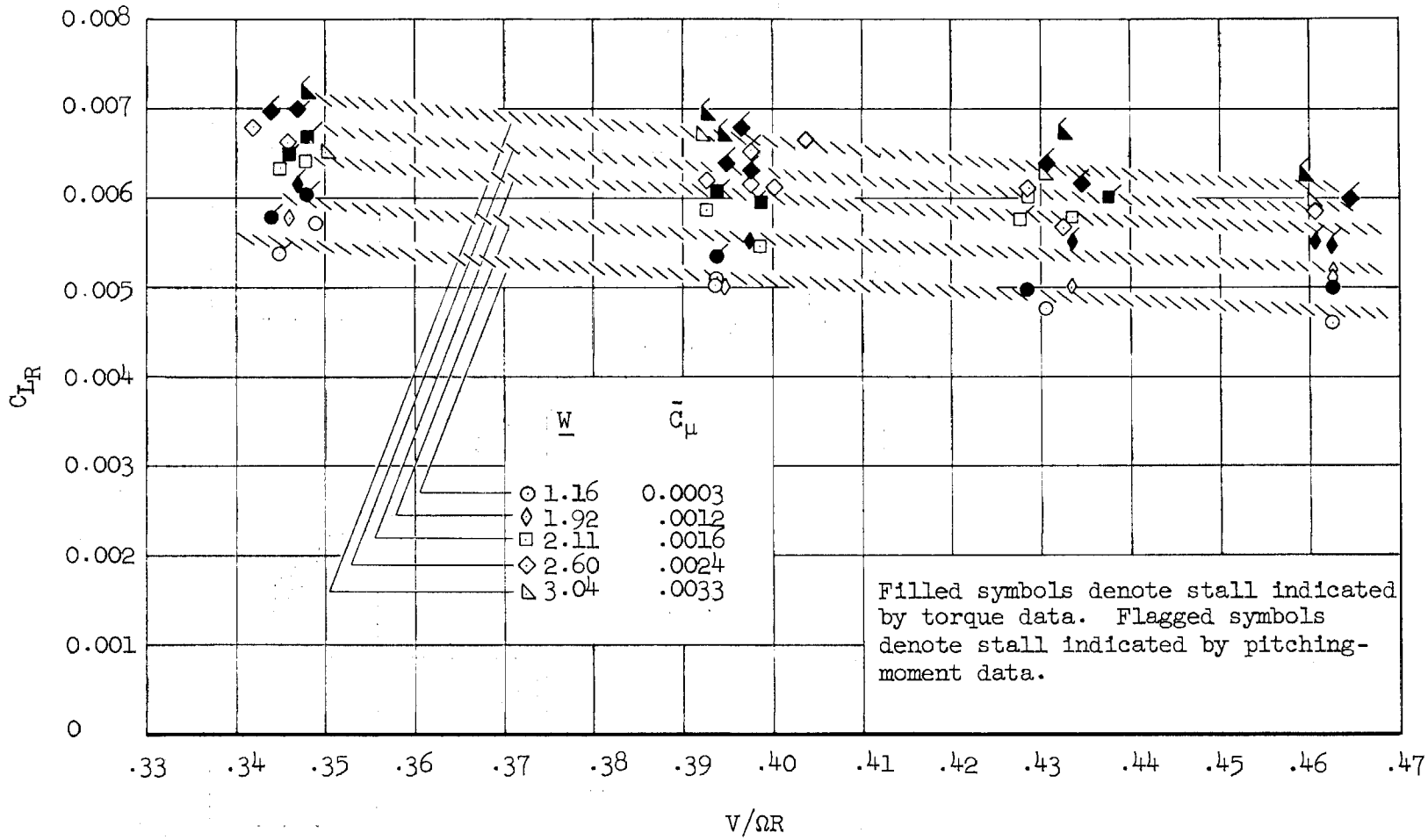

Figure 9.- Stall boundaries for leading-edge boundary-layer-control rotor.

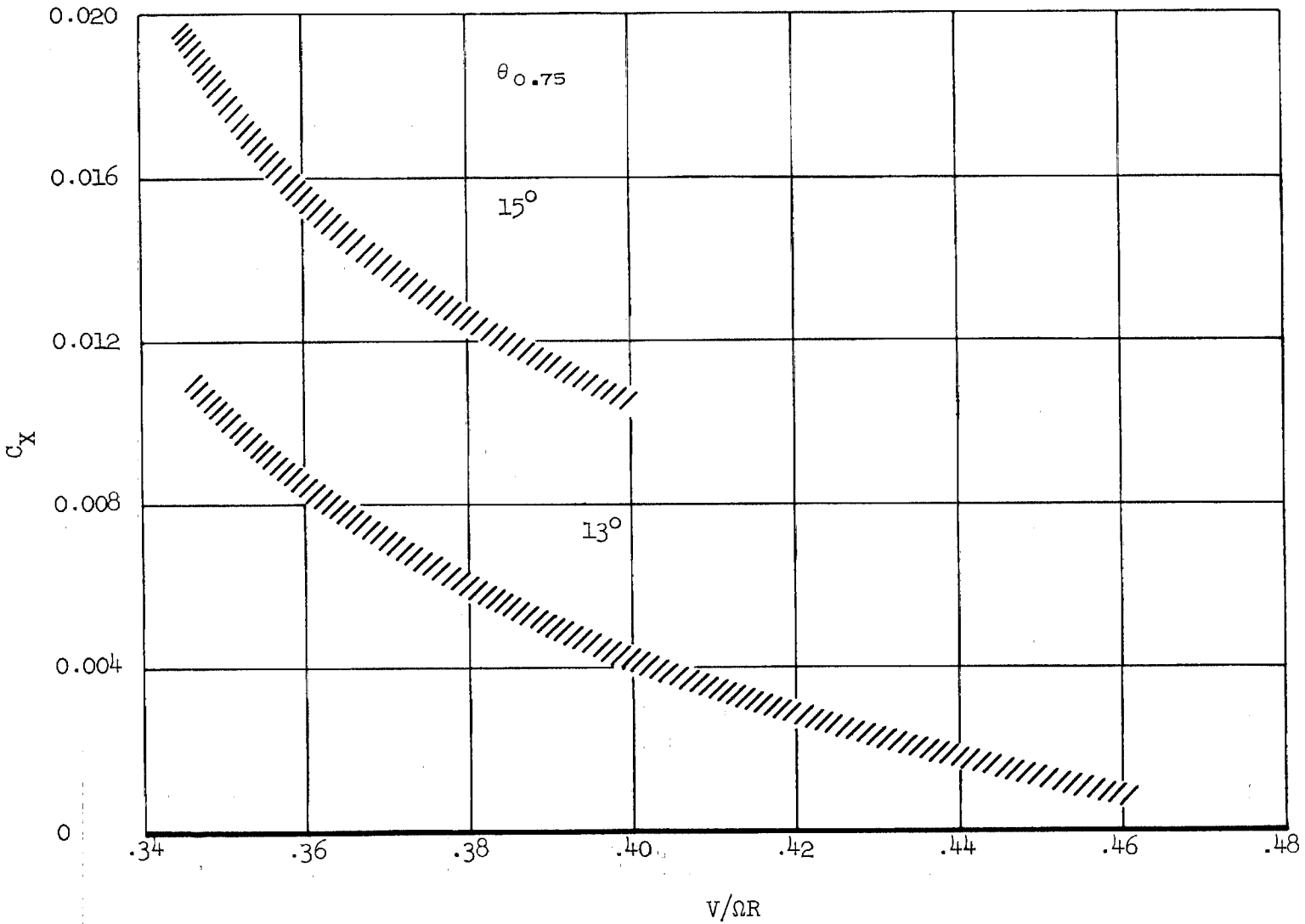

Figure 10.- Longitudinal force coefficient at the stall boundary for leading-edge boundary-layer-control rotor; W = 3.04 lb/sec.

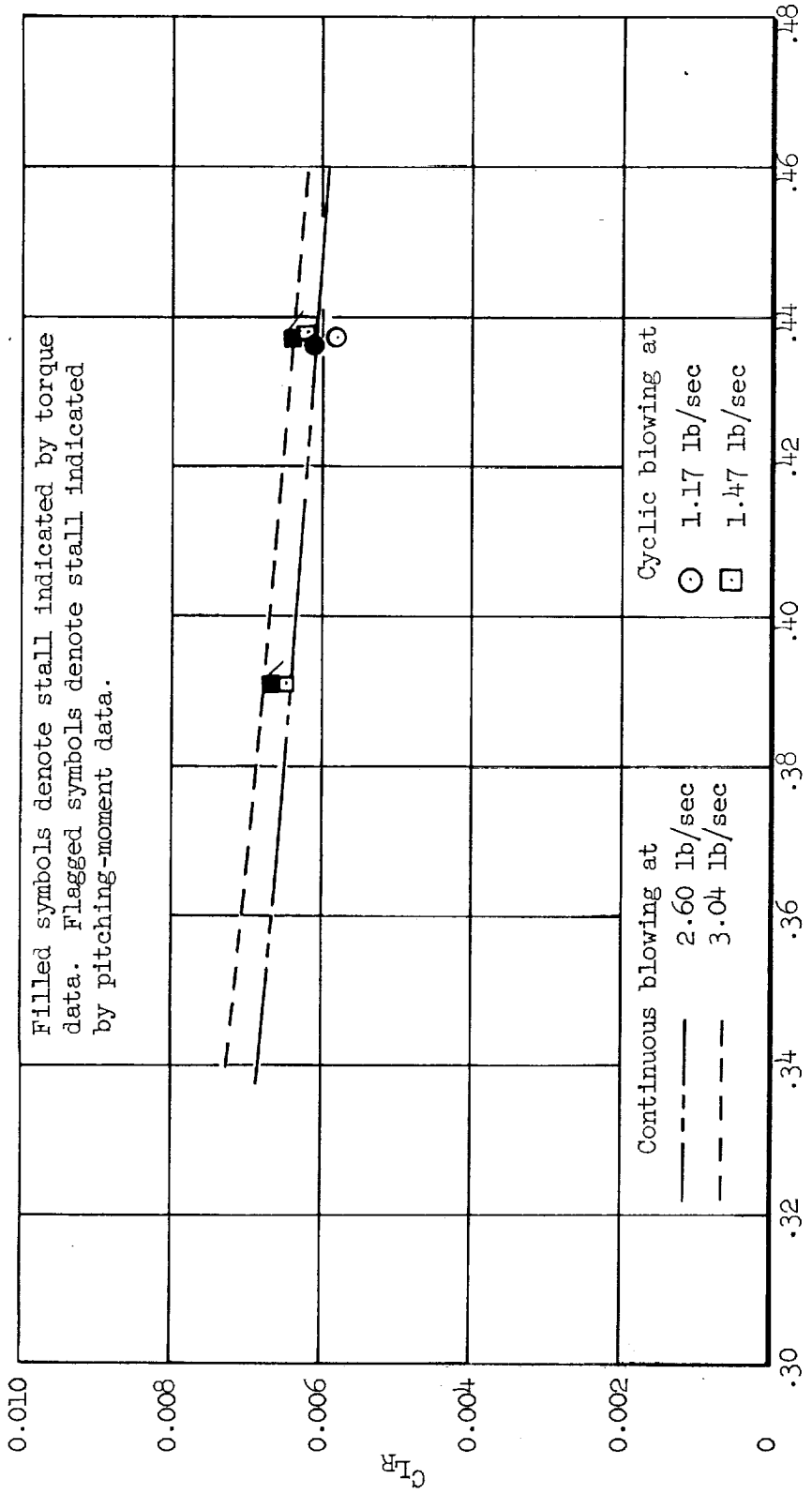

Figure 11.- Comparison of continuous and cyclic blowing stall boundaries for leading-edge boundary-layer-control rotor.

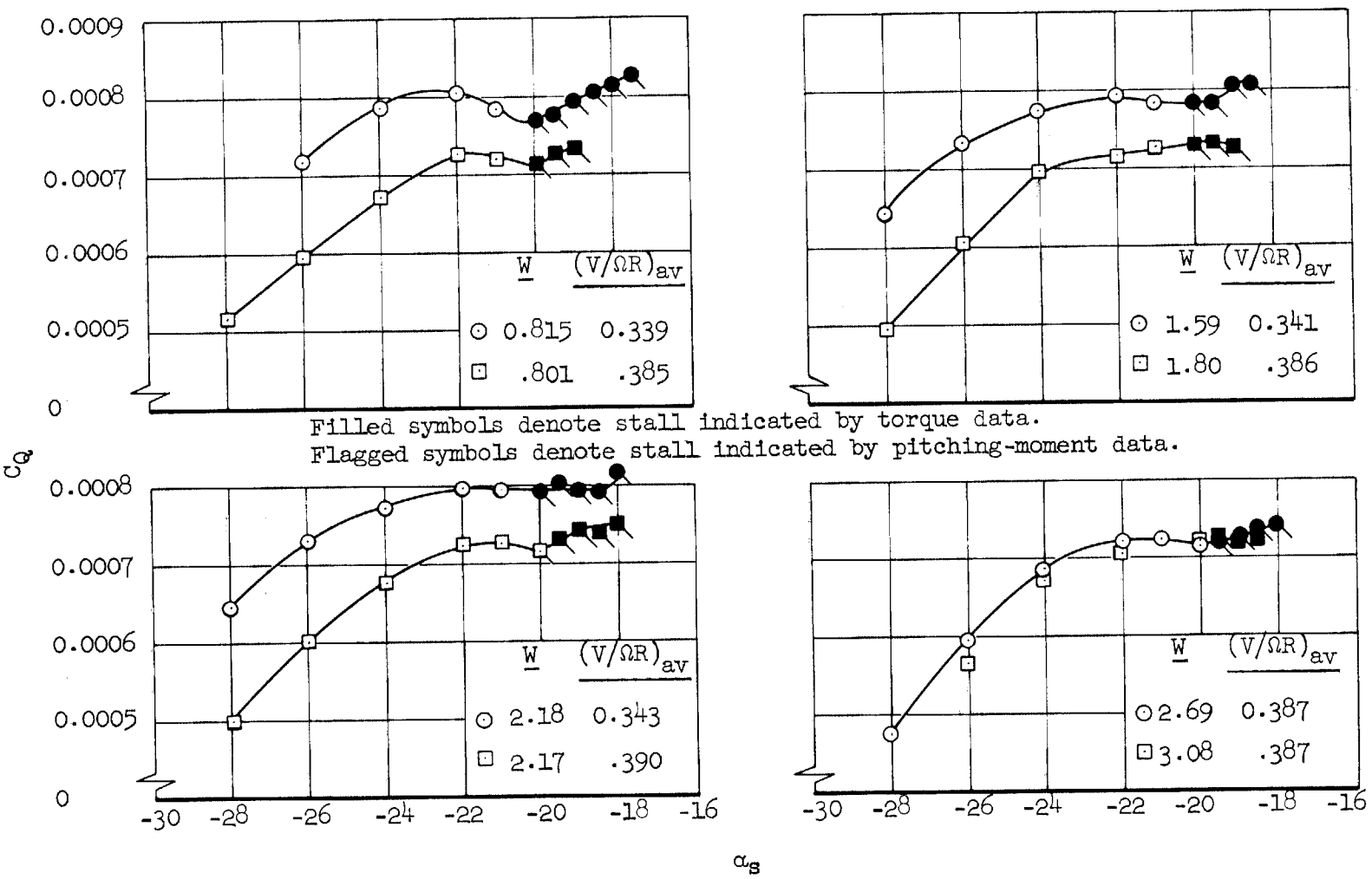

Figure 12.- Torque variation for the mid-chord boundary-layer-control rotor; $\theta_{0.75} = 15^\circ$.

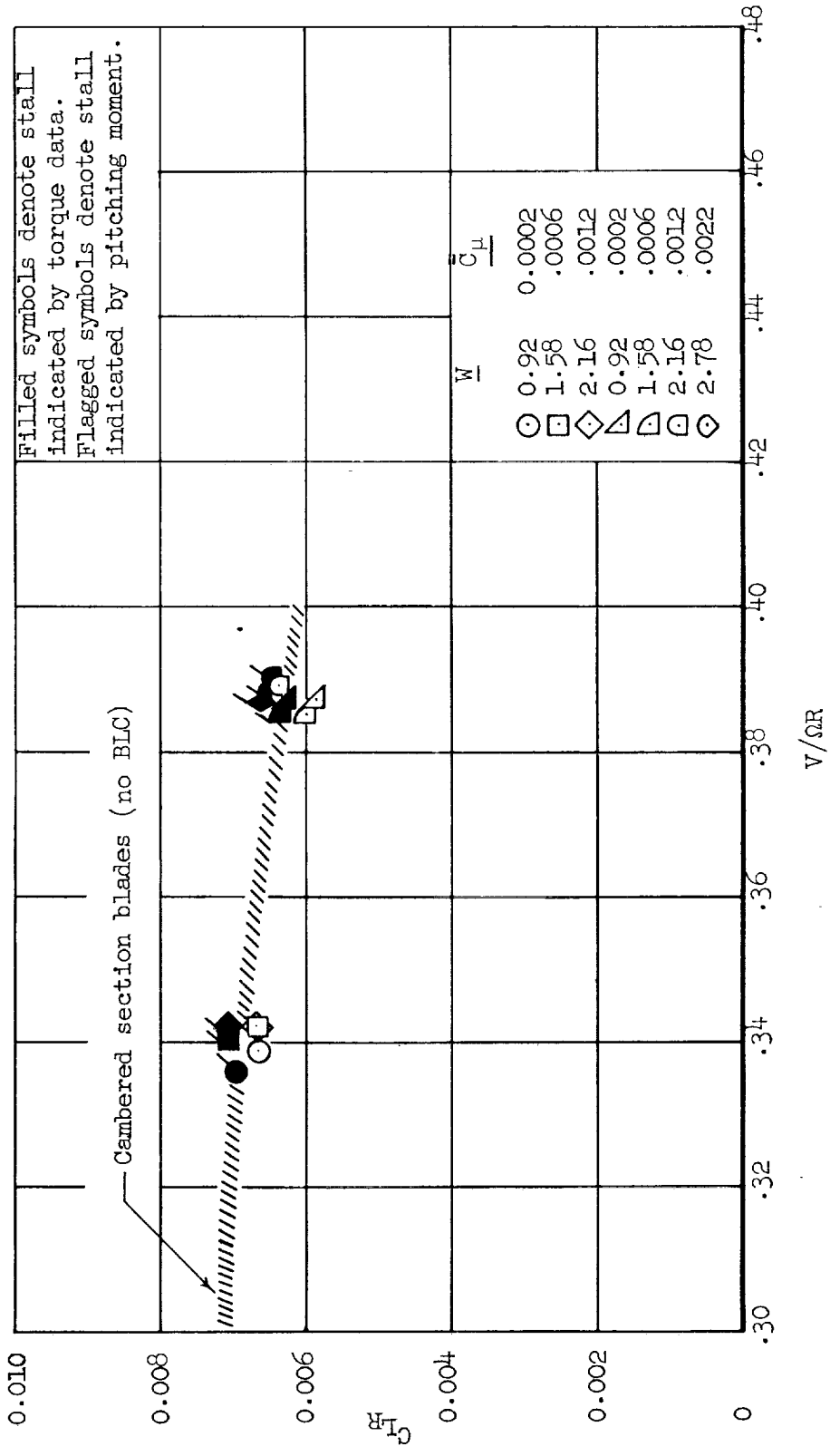

Figure 13.- Stall boundaries for mid-chord boundary-layer-control rotor.

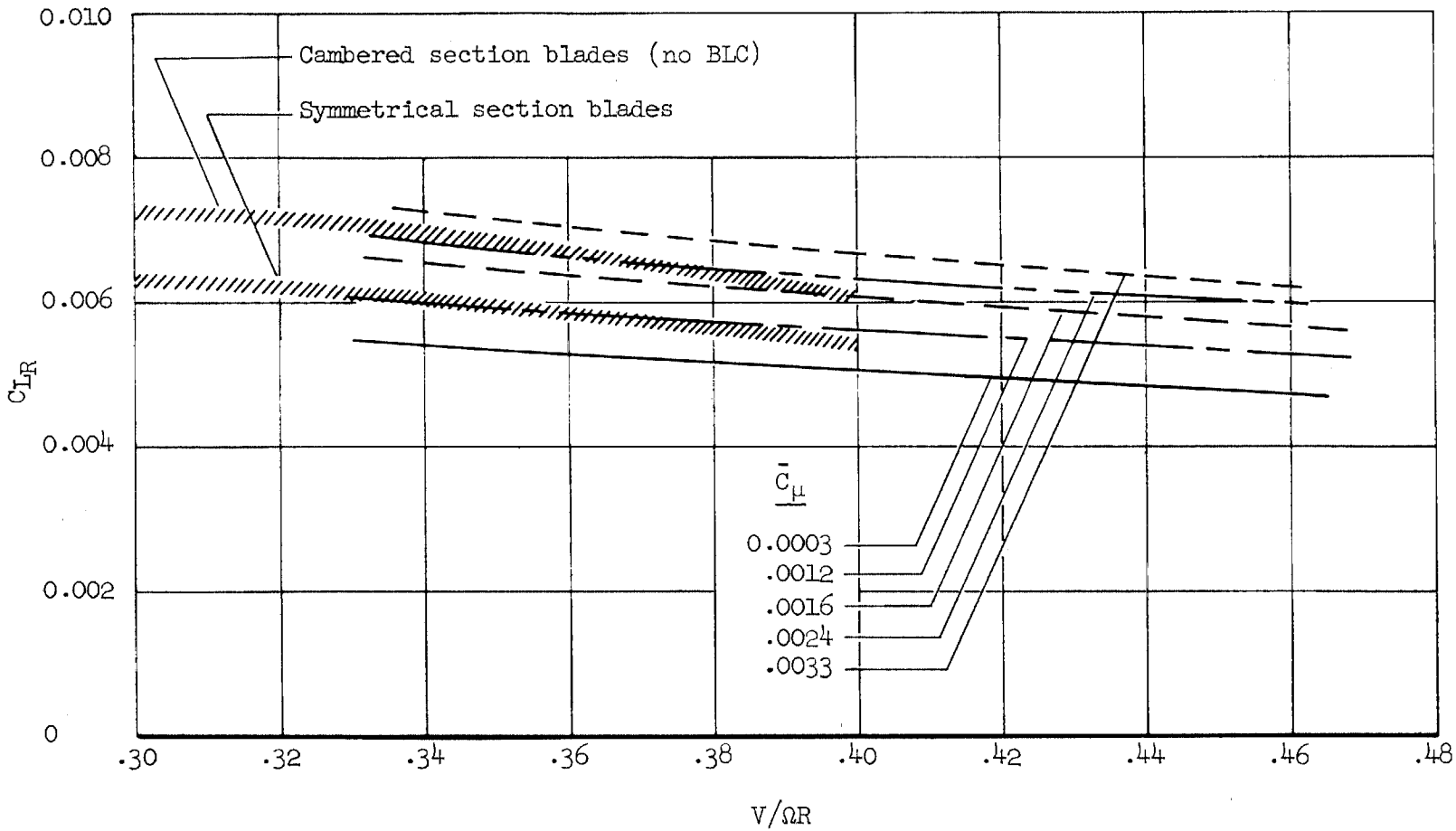

Figure 14.- Comparison of leading-edge boundary-layer-control rotor stall boundaries with those for cambered and symmetrical section rotors of reference 1.

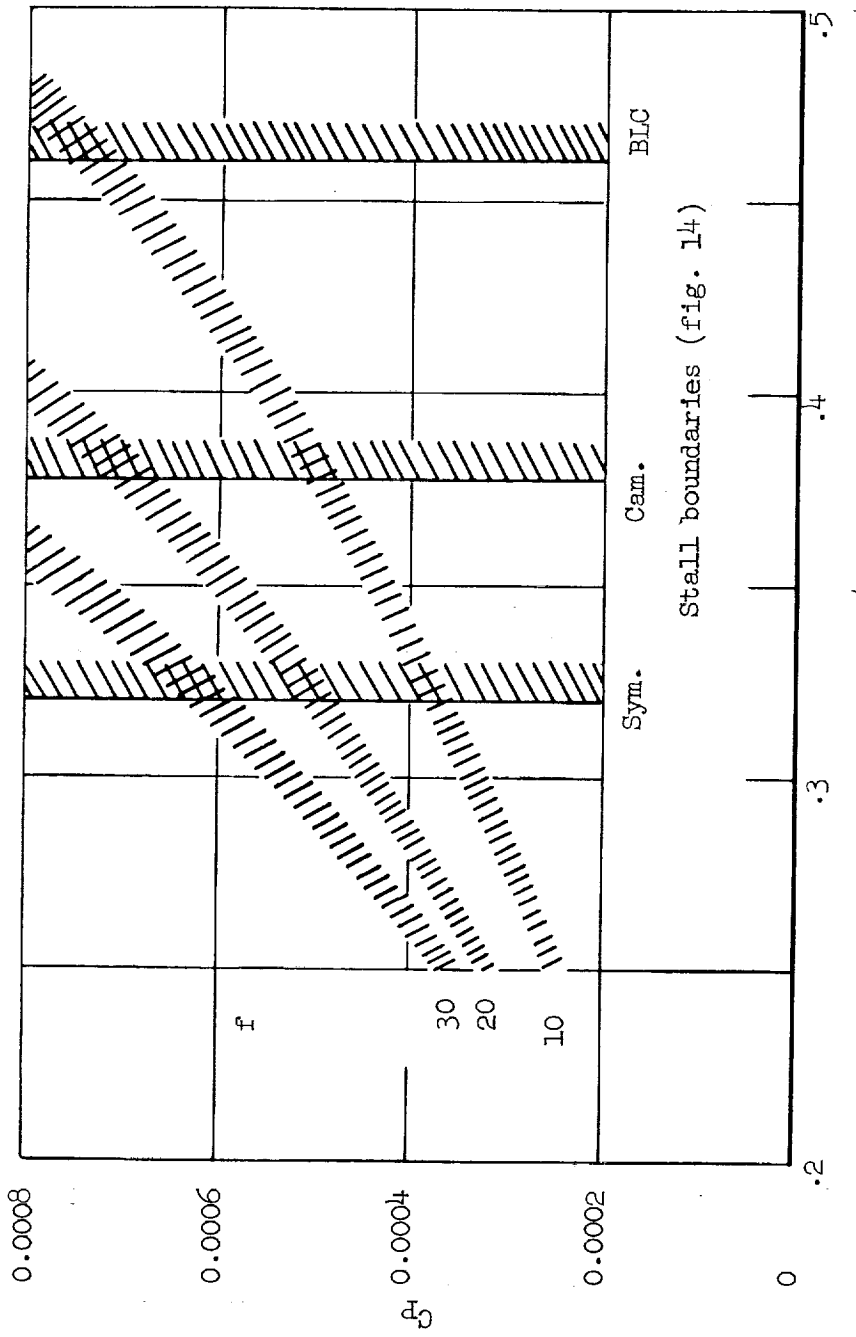

Figure 15.- Approximate shaft power requirements for several fuselage drag loadings; $C_{L_R} = 0.0061$.

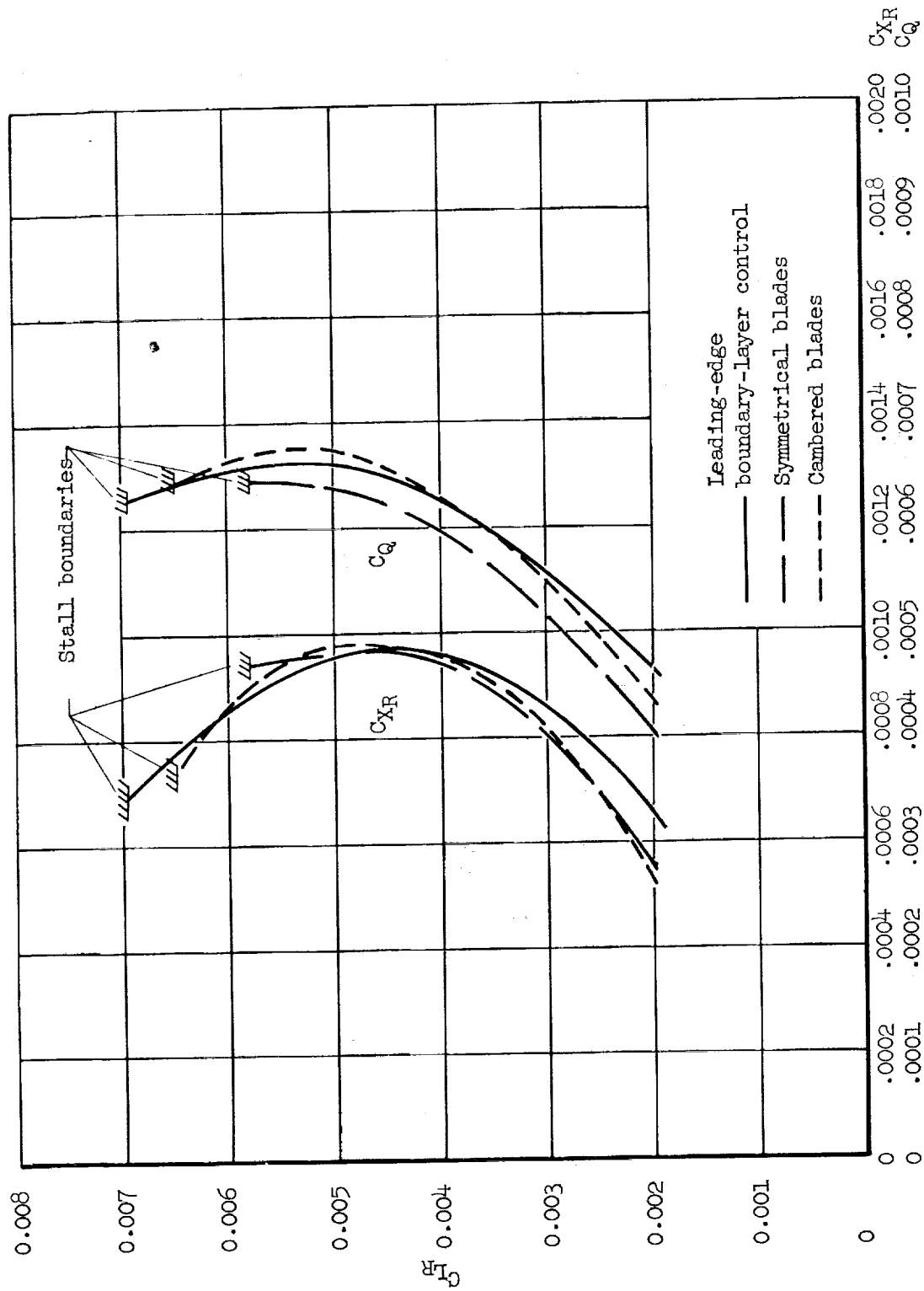

Figure 16.- Comparison of the longitudinal force and torque coefficient; $V/\Omega R = 0.36$.

A

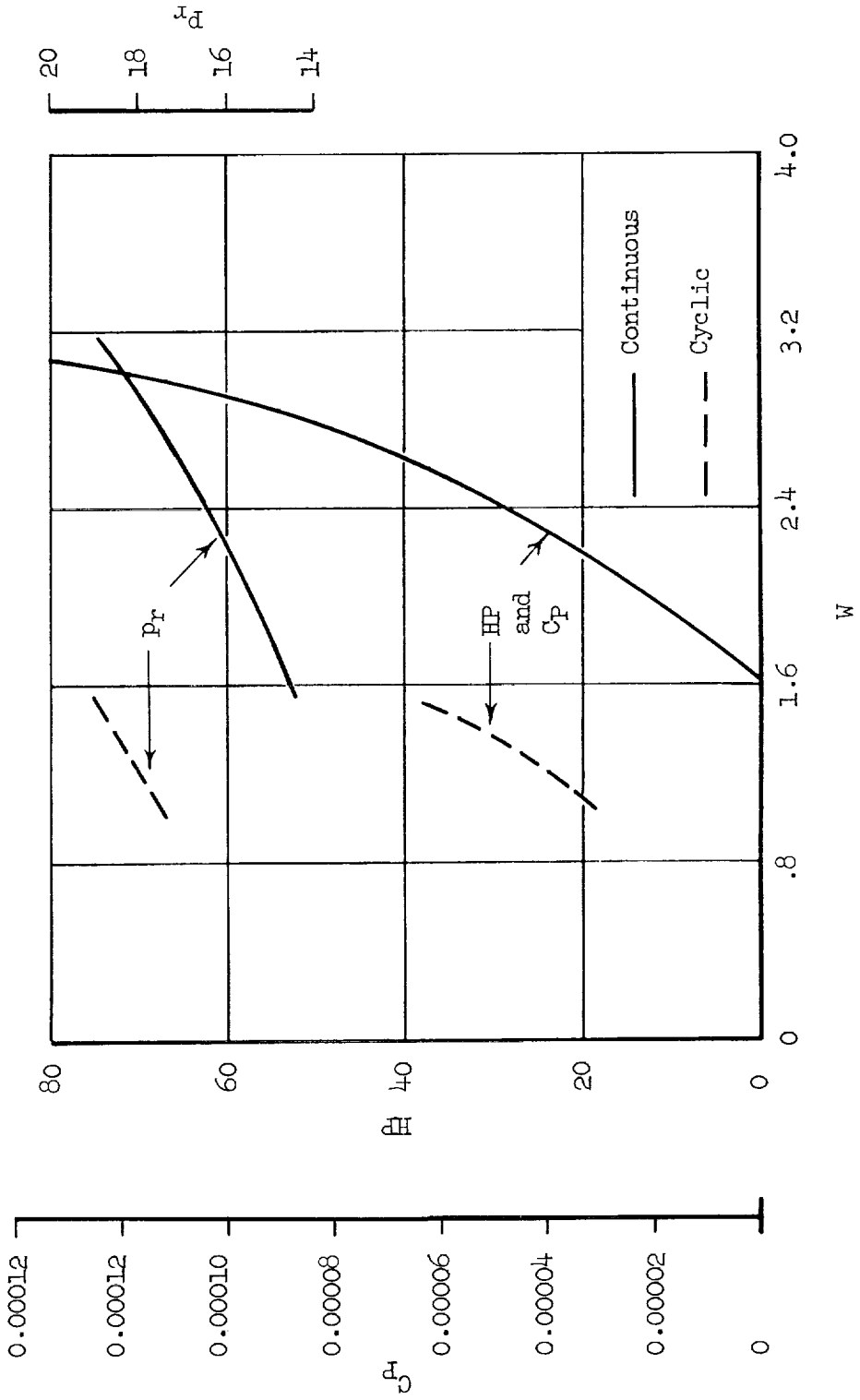

Figure 17.- Calculated air horsepower and blade root inlet pressure for the leading-edge boundary-layer-control rotor with continuous and cyclic blowing.

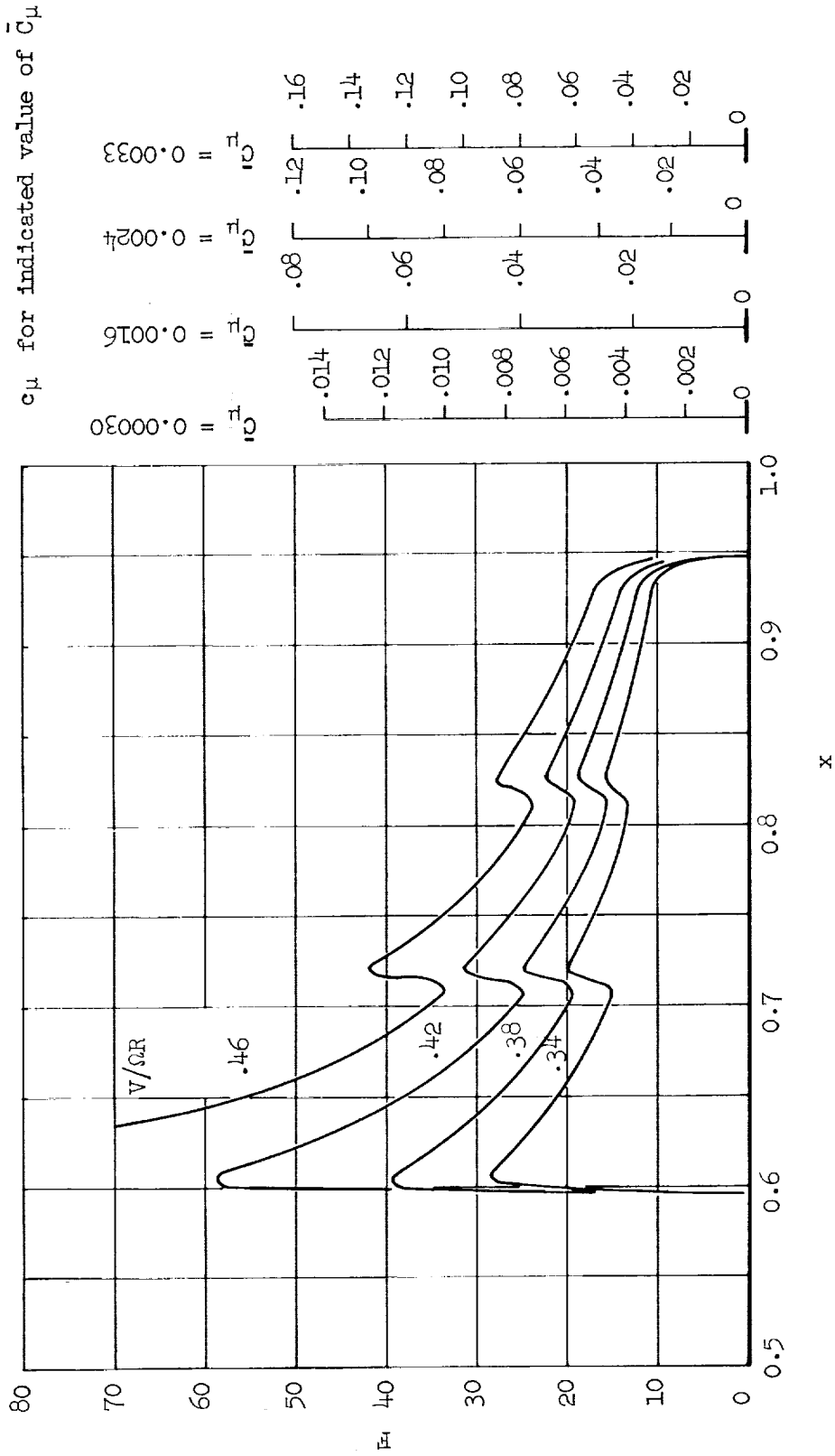

Figure 18.- Radial distribution of momentum coefficient for leading-edge boundary-layer-control blades; $\psi = 270^\circ$.